

Low-dimensional representation of brain networks for seizure risk forecasting

Steven Rico-Aparicio

Physics Department, Industrial University of Santander, Colombia

Martin Guillemaud and Alice Longhena

*Paris Brain Institute (ICM), Inria Paris, INSERM, CNRS,
Sorbonne University, Pitié-Salpêtrière Hospital, Paris, France*

Vincent Navarro and Louis Cousyn

*Department of Neurology, Epilepsy Unit, Pitié-Salpêtrière University Hospital, AP-HP, Paris, France
Center of Reference for Rare Epilepsies, Pitié-Salpêtrière University Hospital, AP-HP, Paris, France and
Paris Brain Institute, Sorbonne Université – CNRS – Inserm, Paris, France*

Mario Chavez*

CNRS, Pitié-Salpêtrière Hospital. Paris, France

Identifying preictal states—periods during which seizures are more likely to occur—remains a central challenge in clinical computational neuroscience. In this study, we introduce a novel framework that embeds functional brain connectivity networks, derived from intracranial EEG (iEEG) recordings, into a low-dimensional Euclidean space. This compact representation captures essential topological features of brain dynamics and facilitates the detection of subtle connectivity changes preceding seizures. Using standard machine learning techniques, we define a dimensionless biomarker, \mathcal{B} , that discriminates between interictal (seizure-free) and preictal (within 24 hours of seizure) network states. Our method focuses on connectivity patterns among a subset of informative iEEG electrodes, enabling robust classification of brain states across time. We validate our approach using a leave-one-out cross-validation scheme and a pseudo-prospective forecasting strategy, assessing performance with metrics such as F1-score and balanced accuracy. Results show that low-dimensional Euclidean embeddings of iEEG connectivity yield interpretable and predictive markers of preictal activity, offering promising implications for real-time seizure forecasting and individualized therapeutic interventions.

I. INTRODUCTION

The characterization of connectivity patterns in complex systems, from brain networks to large-scale infrastructures such as the Internet and social networks, exhibit intricate topologies that require sophisticated analytical frameworks capable of capturing their underlying structure and dynamics [1]. In the context of neuroscience, the study of intracranial electroencephalographic (iEEG) connectivity provides a crucial window into the functional organization of the brain, where network-based approaches have been employed to investigate seizure-related alterations in connectivity [2, 3].

Various computational techniques, including coherence, mutual information, phase synchronization, and transfer entropy, have been applied to iEEG data to quantify neuronal interactions and detect patterns associated with epileptic activity [4]. A key aspect of seizure prediction research relies on comparing interictal (seizure-free) and preictal (before seizures) states to identify early-warning signatures that may precede ictal events [5, 6]. However, one of the major challenges

in this field is selecting an appropriate mathematical framework to represent and analyze brain connectivity networks.

Current approaches to predicting epileptic seizures largely rely on continuous EEG monitoring, using either scalp or intracranial recordings. This strategy demands substantial effort in both data acquisition and analysis. These models focus on detecting seizure-specific preictal patterns but are biased by changes related to shifts in vigilance states. As a result, they require either real-time identification of these states or the incorporation of diverse interictal reference periods.

Recent studies have debated whether Euclidean or non-Euclidean (e.g. elliptic, Gaussian, hyperbolic) embeddings provide a more suitable representation for functional brain networks [7, 8]. While some non-Euclidean (hyperbolic) embeddings have been assumed to be superior in capturing non-trivial (hierarchical or multi-scale) connectivity structures [7], their optimization is prone to numerical difficulties [9]. Moreover, Euclidean embeddings offer a fundamental advantage: they provide an intuitive geometric representation with a well-structured distance metric in a space \mathbb{R}^q , facilitating a more interpretable analysis of embedded data (including the calculation of distances, barycenters and probability distributions).

* e-mail for correspondence: neurodynamicslab@gmail.com

The use of latent geometric representations of anatomical brain networks allowed to identify and quantify the impact of epilepsy surgery on brain regions [10, 11]. In a recent study, we have explored hyperbolic mapping of brain networks to identify discriminative features relevant to seizure prediction [12]. These findings highlight the necessity of integrating network-based approaches to track seizure-related alterations and optimize therapeutic strategies.

Dimensionality reduction techniques play a pivotal role in network analysis, offering a statistical learning approach to condensing high-dimensional connectivity data while preserving essential structural and statistical information. This methodology applies to different brain network analyses, which typically follow a structured pipeline [13]: i) feature extraction: functional connectivity matrices are constructed using synchronization metrics such as the Phase Locking Value (PLV), mutual information, linear or non-linear correlation,...; ii) graph reconstruction: connectivity matrices are transformed into network structures, where nodes represent EEG channels and edges reflect their functional relationships; iii) dimensionality reduction: high-dimensional network data is projected onto a lower-dimensional representation that conveys, with minimal distortion, both local and global geometric information of the original connectivity graph; and iv) classification and prediction: machine learning models are trained to differentiate between different cognitive or neurological states.

This study contributes to the field of computational neurosciences and epilepsy research by presenting a geometric framework that enables the iEEG data representation and classification. This approach strengthens the analytical toolkits for studying epileptic dynamics by enabling the forecasting of state-dependent features and network nodes with high discriminatory value. In contrast to continuous monitoring methods, our strategy aims to assess whether an individual’s iEEG connectivity patterns, recorded during short resting states with controlled vigilance, show differences between interictal (no seizure) and preictal (seizure within the next 24h) periods. We then explore the potential of these patterns to inform daily seizure risk predictions through the use of calibrated forecasting models.

The structure of this article is as follows: we first describe the dataset and preprocessing steps, then detail the embedding and alignment methods, followed by the biomarker formulation and classification strategy. We conclude with a presentation of the classification and forecasting results, and a discussion of their implications in the broader context of network neuroscience and clinical applications.

II. DATA ACQUISITION

The dataset is comprehensively presented in [3]. It consists of daily 10-minute resting-state intracranial EEG (iEEG) recordings from 10 patients (mean age: 30.7 years, mean duration of daily recordings: 11 days) with drug-resistant focal epilepsy, collected between January 2019 and July 2021 at the Epilepsy Unit of Pitié-Salpêtrière University Hospital (Paris, France). The study adhered to the Helsinki Declaration and was approved by an institutional review board (projects C11-16 and C19-55, sponsored by the National Institute of Health and Medical Research).

Each 10-min resting-state period was labeled as “inter-ictal” if no seizure occurred in the next 24h ($N_1 = 69$), or “preictal” if at least one electroclinical seizure occurred in the next 24h ($N_2 = 38$). The implanted regions and the number of electrodes vary between patients ranging between 10 and 62 (median = 20). Details on the demographic information of each patient are available in the original study from this cohort [3].

III. BRAIN NETWORKS CONSTRUCTION

Phase-locking value (PLV) was used to construct connectivity matrices from the iEEG data, which were computed between pairs of EEG signals during 20-second non-overlapping epochs, yielding 30 connectivity matrices per patient day. Synchrony values for the PLV were calculated for typical EEG frequency bands: delta (δ , 1–4 Hz), theta (θ , 4–8 Hz), alpha (α , 8–13 Hz), beta (β , 13–30 Hz), low gamma (low γ , 30–49 Hz), and high gamma (high γ , 51–90 Hz). Only contacts located in the gray matter were considered, and a bipolar montage was applied between adjacent contacts to reduce any spurious synchrony produced by the volume conduction.

Filtering of connectivity matrices

Connectivity matrices represent the degree of synchronization between all pairs of electrodes for one patient, and are analyzed separately for each frequency band. To reduce noise and improve data clarity, a sparse graph is generated from each synchrony matrix, following the method presented in Ref. [14]: PLV matrices are filtered by applying a threshold to cancel a percentage of the weakest values, such that the final networks reached a predetermined mean degree, set here to 3, as recommended for small-size networks. Theoretical and numerical analyses indicate that this filtering method effectively preserves the core structure of weighted graphs, maintaining their hierarchical organization. It enables clear differentiation between groups and facilitates the tracking of rapid temporal changes in network organization [14]. This method reduces the graph to a simplified and sparse form $G = (\Omega, W)$ with

n nodes (i.e number of electrodes implanted) with a weighted matrix $W = \{w_{ij}\}_{i,j \in \Omega}$ that is symmetric and with $w_{ij} > 0$, denoting the PLV value between the pair of electrodes (i, j) .

Euclidean embedding of networks

This study employs an embedding framework within Euclidean space to represent the iEEG connectivity graphs from the preictal and interictal epochs. The Euclidean embedding was chosen to exploit the explicit metric structure inherent to this space, enabling precise quantitative analysis and leveraging the extensive repertoire of well-established statistical parametrization techniques. To achieve dimensionality reduction while preserving the intrinsic data geometry, we adopted the Diffusion Maps algorithm, a method that effectively captures the underlying manifold structure of high-dimensional data [15, 16].

For a connectivity graph G the algorithm estimates the transition probability matrix P of a Markov chain with entries $p_{ij} = \frac{w_{ij}}{d_i}$, where the strength of each node $d_i = \sum_{j \in \Omega} w_{ij}$. Each entry p_{ij} encodes thus the probability of moving from node i to node j through a random walk of length 1. The random walk gives rise to a geometric diffusion with an associated distance between nodes i and j defined as [15, 16]: $d_{ij}^2 = \sum_{k \geq 0} \frac{p_{ik} - p_{jk}}{\mu_k^*}$, where the term μ_k^* denotes the unique stationary distribution of the Markov chain P . By construction, this diffusion distance between nodes is strongly ruled by the connectivity of the graph, and it takes small values if nodes are connected by many paths.

Considering the spectral representations of matrix P , one has a set of eigenvalues $|\lambda_0| \geq |\lambda_1| \geq \dots \geq |\lambda_{N-1}|$ and eigenvectors φ_k and ψ_k such that $\varphi_k^T P = \lambda_k \varphi_k^T$ and $P \psi_k = \lambda_k \psi_k$. The diffusion distance can be written as: $d_{ij}^2 = \sum_{k \geq 1} \lambda_k^2 (\psi_k(i) - \psi_k(j))^2$ where $\psi_k(j)$ denotes the component j of eigenvector k .

The diffusion distance can be approximated to a relative precision using the first q nontrivial eigenvectors and eigenvalues ($\varphi_0 = \mu^*$ and ψ_0 is a constant vector): $d_{ij}^2 \simeq \sum_{n=1}^q \lambda_n^2 (\psi_n(i) - \psi_n(j))^2$. The diffusion map is then constructed as

$$\Psi : x \mapsto \begin{pmatrix} \lambda_1 \psi_1(x) \\ \lambda_2 \psi_2(x) \\ \vdots \\ \lambda_q \psi_q(x) \end{pmatrix}. \quad (1)$$

This mapping $\Psi : \Omega \rightarrow \mathbb{R}^q$ is equivalent to projecting the set of nodes Ω as a cloud of points in an Euclidean lower-dimensional space, where the rescaled eigenvectors and eigenvalues define the spatial coordinates [16]. This process effectively embeds the graph into \mathbb{R}^q such that the diffusion distance between nodes is approximated by the Euclidean distance between their corresponding embedded representations.

An analysis of the eigenvalues derived from the transition matrices P revealed no distinct eigengap that would naturally suggest an optimal embedding dimension q . However, our results show that, on average, the first two nontrivial eigenvectors capture over 80% of the variance associated with the low-dimensional processes underlying brain dynamics. Based on this, we consistently selected $q = 2$ throughout the study. This choice enables a meaningful geometric representation of preictal and interictal states in \mathbb{R}^2 , guided primarily by the need for interpretability and visual inspection of the embedded graphs. The resulting low-dimensional embedding supports a geometric analysis of brain states, facilitates the construction and evaluation of our biomarker \mathcal{B} , and provides a basis for comparison with more complex embedding techniques applied to the same dataset [12]. Although no systematic comparison was conducted across multiple values of q , future studies may evaluate the stability and performance of the method under varying dimensional constraints, and assess whether additional embedding components could significantly contribute to ictal state discrimination.

Diffusion map-based embedding offers the advantage of providing a meaningful representation of the graph, while also defining an explicit distance in the space \mathbb{R}^q that reflects network's connectivity strength. Applied to networks estimated from magnetoencephalographic (MEG) signals, diffusion map embedding allowed to highlight significant differences between the resting-state connectivity structure derived from epileptic patients and those observed in healthy controls [17]. Additionally, in a study with a single patient, an extension of the methodology has been proposed to capture notable spatial shifts in the embeddings of long term iEEG signals, highlighting their potential for detecting changes prior to seizures [18].

Alignment of embedded networks

Prior to comparing groups of embedded networks, we aligned all the projected networks of each patient. This step is crucial, as structurally similar connectivity networks can yield substantially different embedding coordinates, thereby hindering the correspondence of networks across different days [13]. Indeed, the eigenvalue decomposition used in the embedding method can result in coefficient sign flips, rotations, or variations in the ordering of the components. A minor connectivity perturbation may thus result in two embeddings with the same similarities between nodes but with a different structure their coordinate representations [19]. Such effect may artificially inflate the distances between corresponding nodes in embeddings from different days, without reflecting genuine changes in network connectivity. To address this, an alignment procedure was applied to the brain network embeddings within \mathbb{R}^2 , ensuring their comparability across samples.

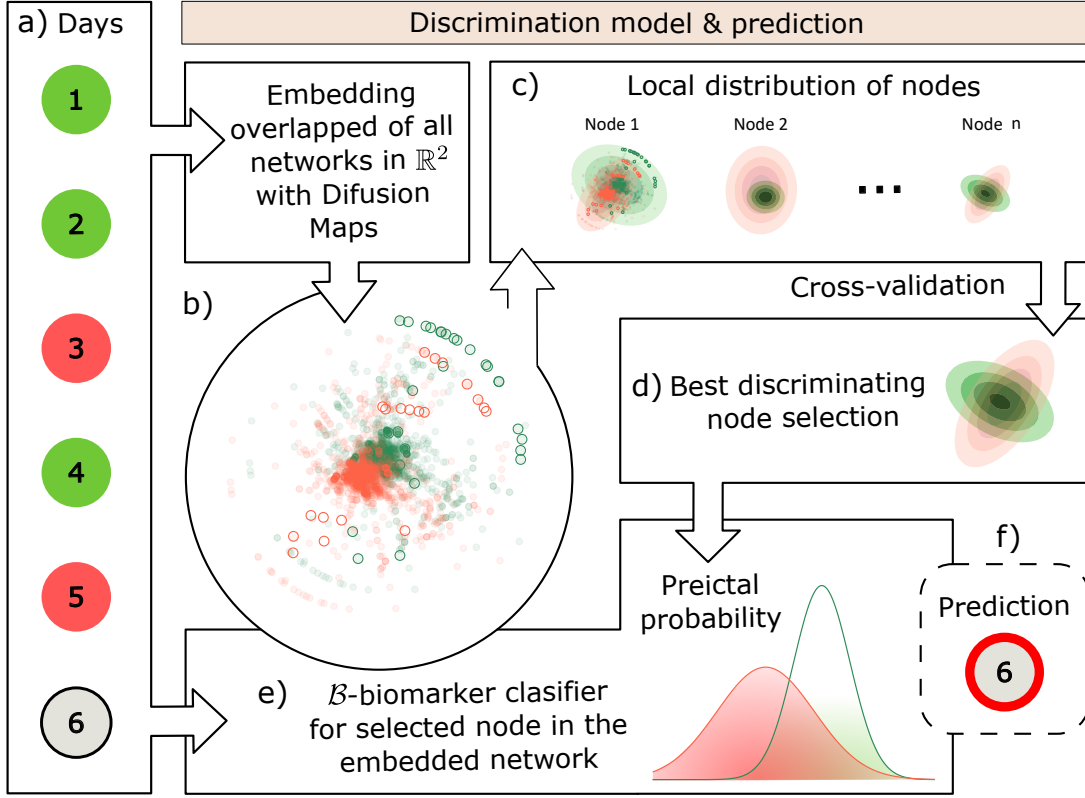


FIG. 1. Illustration of ictal state prediction based on training from previous days, for a given patient and frequency band. The training process follows steps a)–b)–c)–d), and the testing process follows steps e)–f). a) Segments from all days are labeled a priori and color-coded as green (interictal) or red (preictal). b) Each segment is embedded into a two-dimensional Euclidean space using diffusion maps, revealing its characteristic spatial organization. c) For each node, independent Gaussian distributions are estimated for the preictal and interictal states. d) Nodes that exhibit the highest discriminative power between both states are identified through cross-validation. e) In the testing phase, the unknown segment is embedded and classified as preictal or interictal based on the biomarker \mathcal{B} . f) The ictal state of the entire day is determined by averaging the classification outcomes of all segments.

In our study we employed the Procrustes technique as this method modifies the data through translations, rotations, reflections, and scaling, while preserving its main geometric organization [20]. Specifically, we use Generalized Procrustes Analysis (GPA), which belongs to a family of methods designed for analyzing multivariate data to obtain a consensual configuration among several datapoints (here, the embedded networks) [21]. Briefly, GPA transforms a matrix \mathbf{A} of dimension $m \times n$ to be as close as possible to another matrix \mathbf{B} of the same dimensions through the element \mathbf{AT} , where \mathbf{T} is an $n \times n$ matrix that minimizes the trace $\text{tr}[(\mathbf{AT} - \mathbf{B})'(\mathbf{AT} - \mathbf{B})]$. This optimization is achieved through the singular value decomposition (SVD) of the main matrices [22]. The matrix element \mathbf{T} is then defined as $\mathbf{T} = \mathbf{UV}'$.

In our specific case, a set of matrices \mathbf{X} of dimension $n \times 2$ represents n pairs of embedding coordinates in the \mathbb{R}^2 of a network from a single patient. These are transformed to approximate a matrix element \mathbf{Y} of the same dimension, representing a single control segment of the same patient randomly selected from the set of

interictal segments. The transformation is established as $\mathbf{Y}^* = b\mathbf{XT} + \mathbf{C}$. Here, \mathbf{Y}^* is the transformed matrix that minimizes the pointwise distances between the matrices \mathbf{X} and \mathbf{Y} . The scalar b , which accounts for distortion-free scaling of the datasets, is set to $b = 1$. \mathbf{C} is a translation vector determined by the barycenters $\bar{\mathbf{x}}$ and $\bar{\mathbf{y}}$. This non-scaled transformation of a network's nodes is illustrated in Fig. 2.

IV. MODELS FOR EMBEDDED NODES

In this study, to evaluate the potential of preictal states discrimination within the Euclidean space \mathbb{R}^2 resulting from the diffusion map embedding of brain networks, we adopte a local (node-based) perspective. We aim to identify nodes (i.e. electrodes) whose connectivity highlights them as key nodes of interest for preictal state identification.

To achieve this, we performed an aligned embedding in \mathbb{R}^2 of all networks across all interictal and preictal epochs for each patient, effectively creating a superposition

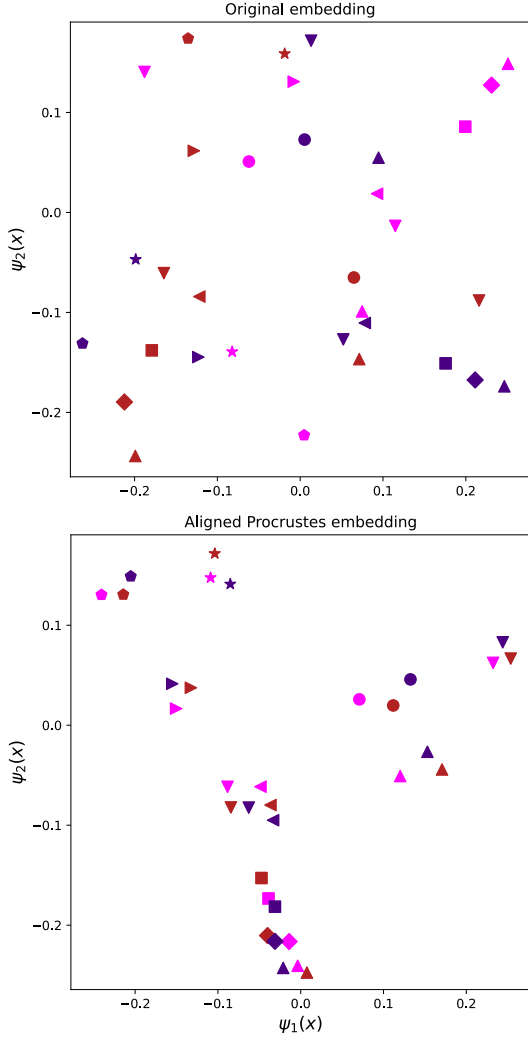


FIG. 2. (Top) Direct Euclidean space embedding of three consecutive networks for patient 5, segment t in red, segment $t + 1$ in magenta, segment $t + 2$ in purple, each segment data contains its respective 11 nodes/electrodes represented by a different figure. (Bottom) Procrustes alignment of the three preictal embeddings with respect to a randomly selected interictal control segment from the same patient.

of $30 \times d \times n$ points projections, where d represents the number of recorded days, each consisting of 30 connectivity networks, where each embedded graph has n points corresponding to n intracranial electrodes. Since a previous study has suggested that the spatial distribution of embedded nodes significantly varies prior to seizure [4], we proceed to locally parameterize and quantify these distributional differences. To this end, we extracted the subset of $30 \times d$ projections for each node to facilitate a comparative analysis between interictal and preictal networks, as illustrated in Fig. 1.

Here, we aimed at detecting nodes from the preictal states as outliers that differ from their distribution observed during interictal baseline. The Bhattacharyya distance was used as a parameter to identify outlier

nodes for each patient. This is an important measure for quantifying the separability between two normal distributions [23]. Since it is a metric in Euclidean space, its interpretation is straightforward: the greater the Bhattacharyya distance, the larger the difference in the spatial nodes' distribution from the nodes' organization during seizure-free epochs. This metric is defined as:

$$D_b = \frac{1}{8}(\boldsymbol{\mu}_2 - \boldsymbol{\mu}_1)^T \left[\frac{\boldsymbol{\Sigma}_1 + \boldsymbol{\Sigma}_2}{2} \right]^{-1} (\boldsymbol{\mu}_2 - \boldsymbol{\mu}_1) + \frac{1}{2} \ln \frac{|\boldsymbol{\Sigma}_1 + \boldsymbol{\Sigma}_2|}{|\boldsymbol{\Sigma}_1|^{1/2} |\boldsymbol{\Sigma}_2|^{1/2}}, \quad (2)$$

where $\boldsymbol{\mu}_i$ and $\boldsymbol{\Sigma}_i$ correspond to the mean vectors and covariance matrices of the preictal and interictal distributions of a given node.

Impact of the alignment

To examine the dependency of this quantification on the selection of the interictal control segment used for alignment, we computed the Z-score value of D_b relative to the surrogate distribution under the null hypothesis that nodes of all networks (interictal and preictal) come from the same distribution. This was ensured by randomly mixing the segments of both states for the patient. The results indicate the presence of preferential nodes that better discriminate between preictal and seizure-free states, as illustrated in Fig. 3.

The alignment step was performed independently for each shuffling iteration, using a different interictal control segment randomly selected from the patient's available interictal original recordings. This strategy avoids introducing alignment bias and ensures that the surrogate distribution of the Bhattacharyya distance D_b captures the variability inherent to the alignment process itself. As a result, the identity of the most discriminative nodes remains highly consistent across iterations. The nodes that exhibit the largest and most significant separation between preictal and interictal states, as measured by the Z scored D_b , consistently emerge across control segments, indicating that their selection is robust to alignment variability.

Preictal biomarker \mathcal{B}

This study proposes the implementation of the parameter \mathcal{B} as the final step for preictal state discrimination, based on the nodal distributions learned from previous interictal and preictal states in each epilepsy patient (Fig. 1). To achieve this, a connectivity network associated with an unknown state is embedded and aligned in the Euclidean space. The point corresponding to the node with the highest discriminative value (previously identified) is compared against the reference nodal distributions of both ictal states. The

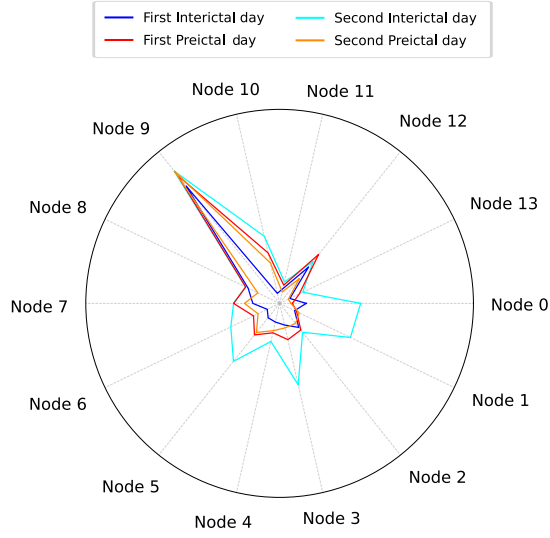


FIG. 3. Mean Z-score values of the D_b distance for 14 nodes, compared to their corresponding surrogate distribution. Displayed for 4 days in the θ band for patient 6.

classification is performed using the evaluation of the multivariate probability density functions (PDF) of that point under each of the two distributions. The PDF of a node \mathbf{x}_j under the distribution $s \in \{\text{interictal}, \text{preictal}\}$ is given by:

$$PDF_s(\mathbf{x}_j) = \frac{1}{(2\pi)^{|\Sigma_i^s|/2}} \exp\left(-\frac{1}{2}(\mathbf{x}_j - \boldsymbol{\mu}_i^s)^T (\boldsymbol{\Sigma}_i^s)^{-1} (\mathbf{x}_j - \boldsymbol{\mu}_i^s)\right)$$

Based on this, we define the proposed dimensionless biomarker as:

Definition of the Dimensionless Biomarker \mathcal{B}

The biomarker \mathcal{B} is a dimensionless parameter that classifies the state of a given network node \mathbf{x} , based on the likelihoods under the preictal and interictal reference distributions.

$$\mathcal{B} = \frac{PDF_{\text{inter}}(\mathbf{x})}{PDF_{\text{pre}}(\mathbf{x})}$$

with the classification criterion of state s given by:

$$s(\mathbf{x}) = \begin{cases} \text{preictal}, & \text{if } \mathcal{B}(\mathbf{x}) \leq 1, \\ \text{interictal}, & \text{if } \mathcal{B}(\mathbf{x}) > 1. \end{cases}$$

Discrimination between interictal and preictal states

The classification of a given network is evaluated using the Leave-One-Out Cross-Validation prediction method, where all segments of the day to be tested are

excluded from the training phase. The full pipeline is applied subsequently, including the embedding of the corresponding connectivity matrices and their alignment with respect to a random control segment. The three most representative nodes of the sample are selected based on their discriminative capacity, and the average of the \mathcal{B} values across these three nodes is computed to determine the predicted class. Sensitivity tests with two, three, and four selected nodes showed no substantial variation in classification metrics, so the choice of three representative nodes was adopted as a balance between robustness and computational simplicity. Each segment is then classified as belonging to either the preictal or interictal class using the biomarker criterion. This process is repeated iteratively across all days for each patient. The classification probability for each day is computed as the proportion of segments labeled as preictal, as shown in Fig. 4.

TABLE I. Discrimination between interictal and preictal resting states: F1 score, and balanced accuracy for all frequency bands.

Band	F1 score	Balanced accuracy
δ	0.52 ± 0.27	0.53 ± 0.14
θ	0.52 ± 0.25	0.55 ± 0.19
α	0.52 ± 0.23	0.52 ± 0.16
β	0.49 ± 0.26	0.50 ± 0.19
Low γ	0.51 ± 0.20	0.51 ± 0.16
High γ	0.60 ± 0.23	0.57 ± 0.12
Best band per patient	0.70 ± 0.23	0.68 ± 0.12

The model's effectiveness in distinguishing preictal from interictal states was assessed using standard classification metrics: the F1-score, and the balanced accuracy. Given the class imbalance in the dataset, where the number of interictal and preictal days is not evenly distributed, the F1-score was selected as a key evaluation metric, as it balances the trade-off between false positives and false negatives. In that order, the balanced accuracy was also calculated, which is defined as the average of sensitivity and specificity, which ensured a fair evaluation of the model's performance across both classes, also mitigating the impact of the dataset's imbalance. The overall classification performance, averaged across all patients and frequency bands, is summarized in Table I.

Daily seizure risk forecasts

Finally, we performed a pseudo-prospective analysis for epilepsy episode prediction. In this forecasting approach, consecutive days were included in the training phase until at least one day of each class was present. The training process identified the three most relevant nodes and computed the biomarker \mathcal{B} to classify each segment of the immediate following day. The predicted class probability of the day was determined by the proportion of segments classified as preictal among the 30 segments

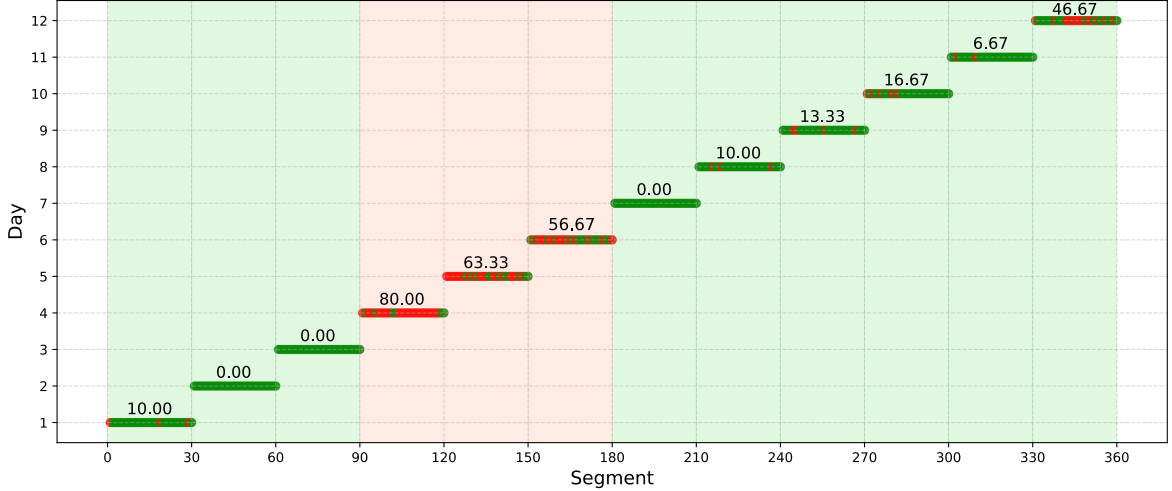


FIG. 4. Leave-one-out cross-validation prediction for patient 8 in the Low γ band. A priori known ictal states are indicated by a colored background, green: interictal, red: preictal - day 4,5,6 -. Each day displays the prediction for its 30 networks obtained from the PLV connectivity matrices. The numerical values represent the percentage of segments predicted as preictal. We classify these percentages as preictal state if $\geq 50\%$, and seizure-free otherwise.

of the predicted day. A threshold of $\geq 50\%$ was used to classify the day as preictal, while lower values were assigned to the interictal state. The results are shown in Fig. 5.

In the case of forecasting, it is found a missing count of true positives or false negatives in some cases, based on this quantification parameters like the accuracy and the Brier score were calculated and are shown in Table II. The accuracy provides a straightforward metric to assess the overall correctness of daily predictions in a range of $[0,1]$ being 1 the most accurate, while the Brier score offers a complementary view by quantifying the probabilistic calibration of the model and the confidence of the classifier in its predictions on a range $[0,1]$ being 0 the most confident.

TABLE II. Pseudo-prospective forecasting of interictal and preictal states: Accuracy and Brier score for all frequency bands.

Band	Accuracy	Brier score
δ	0.55 ± 0.17	0.45 ± 0.17
θ	0.55 ± 0.09	0.45 ± 0.09
α	0.49 ± 0.15	0.51 ± 0.15
β	0.50 ± 0.14	0.50 ± 0.14
Low γ	0.51 ± 0.12	0.49 ± 0.12
High γ	0.49 ± 0.13	0.51 ± 0.13
Best band per patient	0.65 ± 0.14	0.36 ± 0.14

V. RESULTS

The proposed methodology focuses on the localization of discriminating nodes in epilepsy patients through

an Euclidean space embedding, aiming to differentiate between interictal and preictal brain connectivity. Through the calculation of the Bhattacharyya distance between nodal projections and evaluating its statistical relevance through a comparison against shuffled null distributions, it is revealed that a subset of electrodes/nodes consistently exhibits significant geometric reorganization in the Euclidean space (see Fig. 2). Additionally, although the alignment procedure exhibits some sensitivity to the choice of the interictal reference segment, the statistical comparison of nodal distributions across different states demonstrates that the set of discriminative nodes remained consistently robust across recording days for each individual patient, as illustrated in Fig. 3.

Discrimination of preictal states

When classification performance is averaged across all frequency bands and all patients, the F1 score and the balanced accuracy, remain close to random level classification (~ 0.5), as shown in Table I. However, closer inspection of each patient reveals distinct frequency bands where the model is highly discriminant. It becomes clear that some frequency bands allow a better classification on an individual level. For example, as shown in Fig. 4, the model achieved perfect discrimination of seizure and seizure-free days for patient 8 in the Low γ band. To highlight this effect, the last row in Table I shows the average classification metrics computed only on the best-performing frequency band for each patient. This selection results in a notable increase in performance with a high F1 score

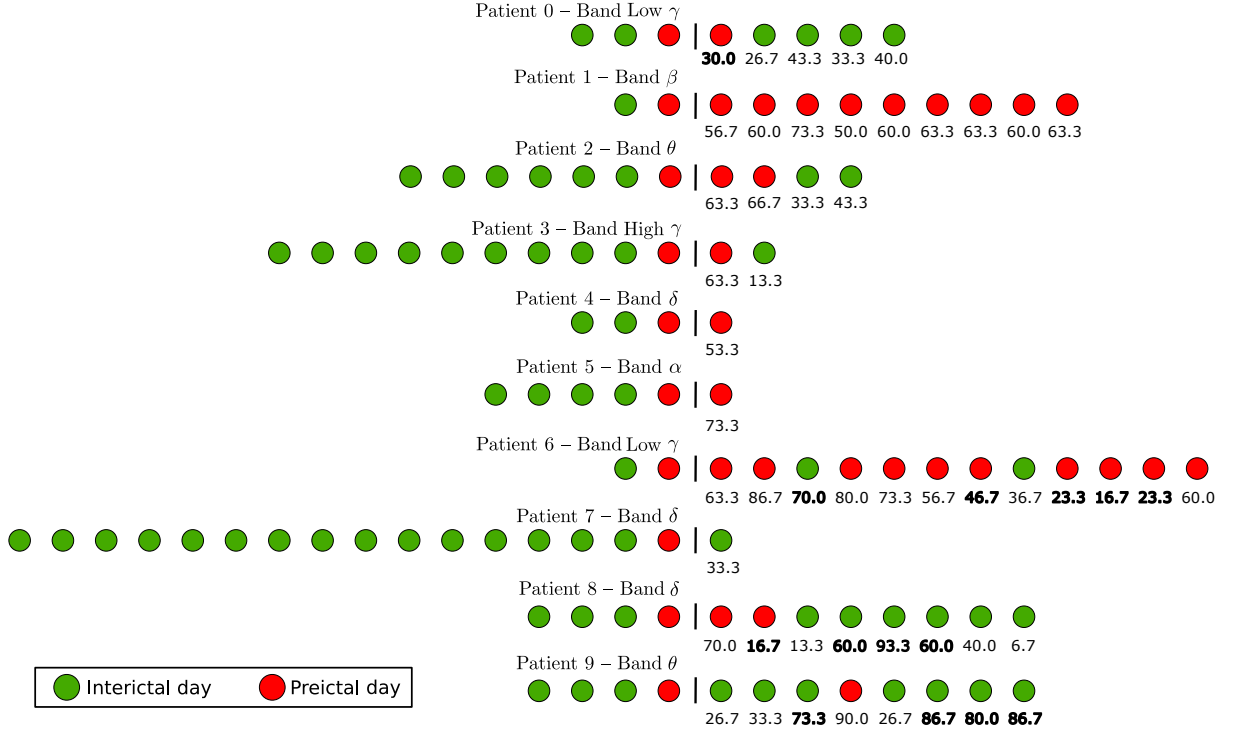


FIG. 5. Forecasting performance in the pseudo-prospective prediction application, where all previous days were used as training to predict the next day. The best performance for each patient is presented with their most discriminative frequency band. Probabilities that failed to predict the correct class are shown in bold.

of 0.70 ± 0.23 and a high balanced accuracy of 0.68 ± 0.12 , suggesting that the proposed method can capture meaningful information for seizure classification when the appropriate spectral band is used.

When applied to the phase-locking values (PLV) estimated between electrodes within the clinically identified seizure onset zone SOZ [3], a standard machine learning model—specifically a support vector machine (SVM)—can achieve an average F1-score of 0.78, and an accuracy of 0.77 [12]. We notice, however, that this model relies on the prior identification of SOZ electrodes.

Forecasting of preictal days

To assess the real-world predictive utility of the proposed biomarker \mathcal{B} , a pseudo-prospective forecasting analysis was conducted following the procedure outlined in Fig. 1. In this framework, the model predicts the ictal state of a given day using only data from preceding days, ensuring that the training set includes at least one day from each ictal class. The global forecasting performance averaged across all patients is shown in Table II. Both the accuracy and Brier score display values close to random classification levels (~ 0.5), similar to the results observed in the global classification task. However, the patient-specific forecasting results shown in Fig. 5 reveal a different picture, demonstrating strong predictive capabilities when the model is applied to

the most informative frequency bands. In particular, 6 out of 10 patients (patients 1, 2, 3, 4, 5, and 7) achieved perfect identification of all seizure and seizure-free days. When the evaluation is restricted to these patient-specific high-performance bands, the classification metrics improve substantially, reaching an average Accuracy of 0.65 ± 0.14 and a low Brier score of 0.36 ± 0.14 , as shown in Table II. In comparison, based on a manual selection of electrodes within the SOZ, the SVM model yields a mean Brier score of 0.13 [3].

From the total of 28 days labeled as preictal, 22 were correctly classified by the proposed forecasting model, yielding a true positive rate (TPR) or sensitivity of 78.57%. For the 23 interictal days, 15 were accurately identified, resulting in a specificity of 65.22%. On the other hand, 8 interictal days were misclassified as preictal (false positives), and 6 preictal days were misclassified as interictal (false negatives). These metrics provide a strong indication that the proposed methodology shows good discriminative capacity of a patient-specific model to anticipate early detection of preictal states, which is the primary goal in seizure forecasting.

VI. DISCUSSION

This study demonstrates that low-dimensional representations of iEEG connectivity networks, derived from daily vigilance-controlled resting-state

recordings, can effectively distinguish between seizure and seizure-free days, offering a reliable and interpretable tool for forecasting daily seizure risk. The use of vigilance-controlled recordings minimizes fluctuations in brain connectivity due to varying alertness levels, thereby enhancing the robustness of preictal state detection. Unlike conventional seizure prediction approaches that rely on continuous long-term EEG monitoring, our results show that brief, daily resting-state sessions are sufficient to capture preictal dynamics at the daily scale [3, 12]. By embedding brain connectivity into a low-dimensional Euclidean space, the proposed methodology further enables the identification of specific network nodes that differentiate interictal from preictal states. This feature holds considerable clinical relevance, as it supports the development of individualized monitoring and intervention strategies aimed at anticipating seizures. Overall, these findings underscore the promise of low-dimensional network embeddings as practical biomarkers for real-time, patient-specific seizure risk assessment.

The proposed model advances seizure forecasting based on brain connectivity analysis within a low-dimensional vector space. While more complex embedding approaches—such as those based in hyperbolic spaces—may offer enhanced predictive performance [12], our results support the effectiveness of low-dimensional embeddings in capturing dynamic changes associated with epilepsy. Notably, this approach achieves performance levels comparable to conventional statistical models, including the support vector machine (SVM) classifier [3]. While the original dataset did not reveal any definitive links between seizure activity and medication tapering [3], the potential impact of timing and treatment modifications cannot be entirely dismissed—an inherent challenge in clinical research. These factors may act as confounding variables and should be carefully considered when drawing interpreting the findings.

Given the well-defined metric structure of Euclidean space, our approach facilitates a more interpretable analysis of network dynamics and seizure-related connectivity changes. Moreover, our results support previous works suggesting that embedding brain connectivity networks into lower-dimensional spaces is sufficient for forecasting seizure risk [12, 18]. However, further research is needed to determine the specific conditions under which other geometrical embeddings may offer advantages, particularly in cases where hierarchical organization plays a dominant role in network connectivity.

Our findings indicate that the most discriminating nodes remain consistent across different days, suggesting that these nodes may play a fundamental role in the neural mechanisms underlying seizure susceptibility. However, classification performance may be influenced by the selection of the interictal reference segment, introducing a potential source of variability. Future

research could explore adaptive strategies for selecting the reference distribution to improve model robustness.

The model’s sensitivity to frequency bands highlights the individualized nature of seizure dynamics where most of the useful discriminant information seems to be contained in the connectivity at the δ , θ and low γ bands. The θ band exhibited one of the highest classification performance across all patients, which aligns with prior studies emphasizing the role of theta oscillations in seizure-related neural activity [3]. The Low γ band also showed one the highest classification results, reinforcing previous observations that fast activity contributes significantly to build a preictal state [12]. Nevertheless, our results suggest that optimal frequency band selection should be tailored to individual patients rather than assuming a universal optimal band.

The pseudo-prospective forecasting approach demonstrated high prediction sensitivity (78.57%), yet exhibited a tendency to misclassify preictal days. Furthermore, false positives were observed in 21.43% of interictal days, indicating that some interictal segments may share connectivity properties with preictal states. This raises the question of whether these misclassifications represent a genuine high susceptibility of seizures.

Beyond classification and forecasting, this methodology contributes to a broader understanding of how brain connectivity changes prior to seizure dynamics. The ability to track network reconfigurations within a low-dimensional space provides new insights into the spatiotemporal evolution of seizure-related activity. Additionally, the patient-specific identification of discriminative nodes suggests the potential for personalized seizure prediction models. Furthermore, characterizing seizure-related changes in connectivity at the level of individual nodes may provide valuable biomarkers for assessing treatment responses in patients undergoing epilepsy surgery or neurostimulation therapy. Nevertheless, given the heterogeneity of electrode location among the patients, we cannot generalize a single unique prediction model. Studies involving significantly larger and more diverse patient cohorts are therefore needed to map out the limits and potential of our seizure risk forecasting.

Overall, this study advances the application of low-dimensional Euclidean embeddings and introduces a biomarker that serves as a promising tool for seizure classification and forecasting. Applied to multimodal recordings, our approach could detect a daily and reliable signature of upcoming seizure(s), offering a broader time window for potential intervention or monitoring throughout the day.

ETHICS

Patients gave written informed consent (project C11-16 and C19-55, conducted by INSERM and approved

by the local ethic committees, CPP Paris VI and Sud Méditerranée 1).

DATA ACCESSIBILITY

The network data that support the findings of this study are available on request from the corresponding author. The raw data are not publicly available due to privacy and ethical restrictions.

AUTHORS' CONTRIBUTIONS

S.R.-A.: investigation, methodology, results visualization, writing—original draft, and editing; M.G.: data curation, investigation, methodology, writing—original draft; A.L.: methodology, writing—original draft; V.N.: data curation, writing—review and editing; L.C.: data curation, methodology, writing—review and editing; M.C.: conceptualization, supervision, result visualization, writing—original draft and editing; All authors gave final approval for publication and agreed to be held accountable for the work performed therein.

FUNDING

This study was supported by the program “Investissements d’Avenir” ANR-10-IAIHU-06, and grants from the “Fondation de l’APHP pour la Recherche - Project PRIAM (Kniazeff Fund)”.

CONFLICT OF INTERESTS

V. Navarro reports fees from Boards with UCB Pharma, EISAI and GW Pharma.

ACKNOWLEDGEMENTS.

S.R.-A. gratefully thanks Luis A. Nuñez for the guidance and mentorship throughout the course of this work, and acknowledges financial support from the ERASMUS+ project, Latin-American alliance for Capacity building in Advance physics (LA-CoNGA physics). M.G. acknowledges doctoral support from the Ecole Normale Supérieure de Lyon, France. A.L. acknowledges financial support from the doctoral school EDITE from Sorbonne University and Inria - Paris.

-
- [1] S. Boccaletti, V. Latora, Y. Moreno, M. Chavez, and D.-U. Hwang, *Physics Reports* **424**, 175 (2006).
 - [2] P. Van Mierlo, M. Papadopoulou, E. Carrette, P. Boon, S. Vandenberghe, K. Vonck, and D. Marinazzo, *Progress in Neurobiology* **121**, 19 (2014).
 - [3] L. Cousyn, R. B. Messaoud, K. Lehongre, V. Frazzini, V. Lambrecq, C. Adam, B. Mathon, V. Navarro, and M. Chavez, *Epilepsia* **64**, e23 (2023).
 - [4] D. Duncan, R. B. Duckrow, S. M. Pincus, I. Goncharova, L. J. Hirsch, D. D. Spencer, R. R. Coifman, and H. P. Zaveri, *Clinical Neurophysiology* **124**, 1943 (2013).
 - [5] R. G. Andrzejak, F. Mormann, T. Kreuz, C. Rieke, A. Kraskov, C. E. Elger, and K. Lehnertz, *Physical Review E* **67**, 010901 (2003).
 - [6] L. Kuhlmann, K. Lehnertz, M. P. Richardson, B. Schelter, and H. P. Zaveri, *Nature Reviews Neurology* **14**, 618 (2018).
 - [7] A. Allard and M. Á. Serrano, *PLoS Computational Biology* **16**, e1007584 (2020).
 - [8] M. Boguna, I. Bonamassa, M. De Domenico, S. Havlin, D. Krioukov, and M. Á. Serrano, *Nature Reviews Physics* **3**, 114 (2021).
 - [9] G. Moreira, M. Marques, J. P. Costeira, and A. Hauptmann, in *Proceedings of the IEEE/CVF Winter Conference on Applications of Computer Vision* (2024) pp. 2082–2090.
 - [10] A. Longhena, M. Guillemaud, and M. Chavez, *Chaos* **34**, 63117 (2024).
 - [11] M. Guillemaud, A. Longhena, L. Cousyn, V. Frazzini, B. Mathon, V. Navarro, and M. Chavez, *Arxiv preprint 10.48550/arXiv.2412.17820* (2024).
 - [12] M. Guillemaud, L. Cousyn, V. Navarro, and M. Chavez, *Physical Review Research*. In press (2025).
 - [13] J. Richiardi, S. Achard, H. Bunke, and D. Van De Ville, *IEEE Signal Processing Magazine* **30**, 58 (2013).
 - [14] F. De Vico Fallani, V. Latora, and M. Chavez, *PLoS Computational Biology* **13**, 1 (2017).
 - [15] R. R. Coifman and S. Lafon, *Applied and Computational Harmonic Analysis* **21**, 5 (2006).
 - [16] S. Lafon and A. B. Lee, *IEEE Transactions on Pattern Analysis and Machine Intelligence* **28**, 1393 (2006).
 - [17] M. Chavez, M. Valencia, V. Navarro, V. Latora, and J. Martinerie, *Physical Review Letters* **104** (2010).
 - [18] D. Duncan, R. Talmon, H. P. Zaveri, and R. R. Coifman, *Mathematical Biosciences & Engineering* **10**, 579 (2013).
 - [19] F. Gürsoy, M. Haddad, and C. Bothorel, *Neurocomputing* **553**, 126517 (2023).
 - [20] J. C. Gower, *Psychometrika* **40**, 33 (1975).
 - [21] G. B. Dijkstra and J. C. Gower, *Food quality and preference* **3**, 67 (1991).
 - [22] C. M. Cuadras, *Nuevos métodos de análisis multivariante*, Vol. 20 (CMC editions Barcelona, 2007).
 - [23] K. Fukunaga, *Introduction to statistical pattern recognition* (Elsevier, 2013).